

RESEARCH

Open Access



Seasonal variations in aerosol characteristics from local pollution and long-range transport at the northern tip of Taiwan

Tse-Lun Chen¹, Wei-Jen Hsieh², Hsin-Chih Lai³, Neng-Huei Lin², Si-Chee Tsay⁴, Charles C. K. Chou⁵ and Ta-Chih Hsiao^{5,6*} 

Abstract

Understanding aerosol characteristics and their influence on cloud condensation nuclei is essential for clarifying the connections between regional air pollution and global climate change. Asian continental outflows, laden with significant anthropogenic emissions, can profoundly affect local air quality. This study examines local pollution (LP) and long-range transport (LRT) events at Cape Fuguei, Taiwan's northernmost point, during the spring and autumn seasons from 2014 to 2016. We utilized a multi-pronged approach that integrates in-situ measurements, back-trajectory analysis, and satellite observations to differentiate between LP and LRT events and assess their pollutant profiles. Our findings indicate notable distinctions: LRT events, primarily driven by northeastern winds, display higher activation ratios and lower black carbon (BC) ratios compared to LP events. Seasonal variations were pronounced, the activation ratios and geometric mean diameter show a stronger positive correlation during autumn LRT events compared to spring events, suggesting increased particle aging during transport. Wind direction played a crucial role in determining pollutant characteristics. Southwestern winds were associated with higher BC concentrations, indicative of LP sources, while northeastern winds during the autumn/winter monsoon were linked to LRT events with potentially more complex aerosol aging processes. These findings underscore the importance of considering both local and long-range sources in air quality assessments and the potential impacts of changing regional emission patterns on local air quality.

Keywords Cloud condensation nuclei, Activation ratio, Long-range transport, Eastern Asian continental outflow, Seasonal variation

1 Introduction

Transboundary or long-range transport (LRT) of air pollution is a significant contributor to haze episodes across inland and coastal regions of Asia [1]. Typically observed from late autumn to early spring, the movement of cold high-pressure systems from Siberia, combined with northeast (NE) monsoons, facilitates the transport of polluted air masses across East Asia, affecting countries like China, Korea, Japan, and Taiwan [2–8]. The northern tip of Taiwan, such as Cape Fuguei, situated downstream of this continental outflow and separated by mountains, serves as a crucial point for assessing transboundary

*Correspondence:

Ta-Chih Hsiao
tchsiao@ntu.edu.tw

¹ Institute of Environmental Engineering, National Sun Yat-Sen University, Kaohsiung 804201, Taiwan

² Department of Atmospheric Sciences, National Central University, Taoyuan 320317, Taiwan

³ Department of Green Energy and Environmental Resources, Chang Jung Christian University, Tainan 711301, Taiwan

⁴ NASA Goddard Space Flight Centre, Greenbelt 20771, USA

⁵ Research Centre for Environmental Changes, Academia Sinica, Taipei 115201, Taiwan

⁶ Graduate Institute of Environmental Engineering, National Taiwan University, Taipei 106319, Taiwan



© The Author(s) 2025. **Open Access** This article is licensed under a Creative Commons Attribution 4.0 International License, which permits use, sharing, adaptation, distribution and reproduction in any medium or format, as long as you give appropriate credit to the original author(s) and the source, provide a link to the Creative Commons licence, and indicate if changes were made. The images or other third party material in this article are included in the article's Creative Commons licence, unless indicated otherwise in a credit line to the material. If material is not included in the article's Creative Commons licence and your intended use is not permitted by statutory regulation or exceeds the permitted use, you will need to obtain permission directly from the copyright holder. To view a copy of this licence, visit <http://creativecommons.org/licenses/by/4.0/>.

pollution during the NE monsoon season [9, 10]. These outflowing air masses often carry dust and $PM_{2.5}$ (particulate matter with a diameter of 2.5 μm or smaller), which includes hygroscopic chemical compositions [11, 12]. During the NE monsoon season, air pollutants in East Asia are transmitted over long distances to Taiwan. It was found that air masses from mainland China contribute the most to $PM_{2.5}$ levels in northern Taiwan, reaching up to 80% from winter to spring [13]. During the winter of 2017, it was found that the average mass fractions of SO_4^- and NO_3^- mixed within $PM_{2.5}$ chemical compositions were 7 ± 13 and $11 \pm 15\%$, respectively, while the aerosol mixing state continued to exhibit diversity even after regional pollution was transported over distances of 500 to 1000 km [14]. During the COVID-19 lockdown in China, the concentration of NO_2 decreased by 24% compared to the same period in previous years, resulting in a significant reduction in $PM_{2.5}$ concentrations reaching Taiwan [15, 16]. Simulation studies indicate that $PM_{2.5}$ concentrations from LRT transport can peak between 45 to 100 $\mu\text{g m}^{-3}$ during haze episodes [7, 17]. Furthermore, LRT from East Asia is frequently laden with anthropogenic sulfate and nitrate particles, particularly during the monsoon season [18]. Local pollutants may interact with these transported plumes, complicating the atmospheric mixture and contributing to secondary aerosol formation [18, 19], especially observed in northern urban areas of Taiwan [20].

Aerosol hygroscopicity plays a crucial role in influencing both regional and global climates, as it affects cloud condensation nuclei (CCN) and cloud formation processes. The hygroscopicity of aerosols depends on their chemical composition and particle size. Newly formed and aged aerosol particles can absorb organic and sulfuric vapors, enhancing their size and increasing CCN concentrations [21, 22]. Higher CCN concentrations can lead to increased cloud albedo, impacting the Earth's radiation budget [23]. Smaller cloud droplets may inhibit low cloud formation and short-lived rainfall [24–26], while larger CCN can enhance precipitation in convective clouds [27]. Aerosols rich in hygroscopic materials can lower the supersaturation (SS) needed for vapor condensation, facilitating cloud droplet formation. However, measuring aerosol hygroscopicity in ambient environments remains challenging compared to laboratory settings [28]. An SS of 0.1% suggests the maximum expected influence of chemical composition, while 0.4% indicates conditions favorable for the formation of convective clouds. In contrast, an SS of 0.8% reflects a highly supersaturated environment, where nearly all aerosols are likely to activate as CCN [29]. The ambient observations made off the Californian coast have shown that in clean marine air, SS levels often surpass 1% [30]. In urban areas, aerosols

with low hygroscopic materials, such as soot, can diminish overall hygroscopicity [31]. Conversely, low wind speeds (WS) can enhance moisture uptake in the presence of water-soluble inorganic ions, leading to size growth—a phenomenon known as aging [32–35]. Factors influencing aerosol hygroscopicity include chemical composition, environmental conditions, emission sources, mixing states, and aging processes. In situ measurements of aerosols' physicochemical properties are vital for understanding their hygroscopicity effects [36, 37].

The seasonal variations in aerosol characteristics and their impacts on CCN activity have been increasingly recognized as critical factors in understanding air quality and climate interactions. Research has shown substantial seasonal differences in aerosol physicochemical properties, influenced by meteorological conditions, emission patterns, and atmospheric chemistry [38]. The transition from winter to spring in East Asia is marked by frequent LRT events, while summer to autumn transitions often involve a mix of local and transported pollutants. Such seasonal shifts can lead to changes in particle size distributions, chemical composition, and hygroscopicity, ultimately affecting CCN activity and cloud formation processes [39]. Understanding these seasonal dynamics is essential for accurate climate modeling and effective air quality management.

To quantify LP and LRT pollutants, trajectory statistics and chemical transport models are commonly used. The former calculates emissions frequency based on backward trajectories, while the latter simulates emissions from specific areas. Both methods face uncertainties due to variabilities in emissions, chemical reactions, and meteorological conditions [40]. However, field measurements can provide valuable data to support these simulations. This study utilizes the spring (March to April) and autumn (October to November) seasons in a consecutive three years (2014–2016) of ground-based measurements, along with analysis of backward trajectories and aerosol optical depth (AOD) from satellite data, to characterize the CCN activation ratio (AR) and pollutant characteristics during LRT. By focusing on these transitional seasons, we aim to elucidate the complex interplay between local and long-range transported pollutants, their seasonal variations, and their impacts on CCN activity. This approach allows us to address critical gaps in our understanding of aerosol-cloud interactions in a region significantly affected by both local emissions and transboundary pollution.

2 Methods

2.1 Measurement site and instrumental set-up

Our approach to identifying and characterizing LRT and LP events combined in-situ measurements, local

monitoring station data, back-trajectory analysis, and satellite observations. This multi-pronged strategy enabled a thorough assessment of air mass origins and properties at Cape Fuguei (25.30° N, 121.54° E), as shown in Fig. S1. This site is strategically positioned to monitor the influence of the Asian continental outflow on air quality [6, 41]. Taiwan's distinct seasonal meteorological patterns play a significant role; during winter and autumn, the northeastern monsoon exacerbates air pollution with increased rainfall and stronger winds. In contrast, spring and summer see a rise in LP from southern flows [14, 42, 43]. Although spring experiences orographic rain, most rainfall occurs during the plum rain season, leading to unstable weather and greater temperature fluctuations. The northeastern monsoon typically transports pollutants from Northeast Asia to Taiwan, highlighting Cape Fuguei's importance for monitoring pollution. Data collection took place in three periods: spring 2014 (Mar. 4 to Apr. 13), autumn 2015 (Oct. 26 to Nov. 12), and autumn 2016 (Oct. 17 to Nov. 30), acknowledging that emissions during these times may differ from winter patterns.

The PM_{2.5} mass concentration was measured using a Tapered Element Oscillating Microbalance (TEOM, Model 1405 F, Thermo Fisher Scientific) operating at a flow rate of 16.67 L min⁻¹. A 7-wavelength Aethalometer (AE33, Magee Scientific, USA) was employed to directly estimate the black carbon (BC) mass concentration with aerodynamic diameter of 2.5 μm at measurement wavelength of 880 nm. The particle number size distribution was determined using a scanning mobility particle sizer (SMPS, Model 3936, TSI), which was equipped with an electrostatic classifier and a butanol-based condensation particle counter (Model 3010, TSI). The geometric mean diameter (GMD) and BC ratio were identified in Eqs. (1) and (2):

$$\text{GMD}(d_g) = \exp \frac{\sum_i (\ln d_{pi}) \times N_i}{\sum_i N_i} \quad (1)$$

$$\text{BC ratio (\%)} = \frac{\text{BC mass concentration}}{\text{PM}_{2.5} \text{ mass concentration}} \times 100 \quad (2)$$

In addition, the CCN activity was assessed with a CCN counter (CCNC-100, DMT) at a flow rate of 0.5 L min⁻¹. The AR, which signifies changes in aerosol hygroscopicity potentially influenced by particle size and composition, was computed using the number concentrations of condensation nuclei (N_{CN}) and CCN (N_{CCN} measured at the SS of 0.4%), as demonstrated in Eq. 3. We chose 0.4% SS as it represents a typical value for aerosol particles activated as CCN, allowing researchers to study the behavior of these particles under conditions similar to those found in natural clouds [38]. An increase in the AR value signals

a higher likelihood of CCN formation. A more hygroscopic particle corresponds to a smaller activation energy barrier necessary for particle growth — conversely, particles with weaker hygroscopicity yield lower AR values.

$$\text{AR} = \frac{N_{CCN}}{N_{CN}} \times 100\% \quad (3)$$

2.2 Multi-criteria approach for identifying LRT events

We employed a comprehensive, multi-criteria approach to robustly identify and distinguish between LRT and LP events. This strategy integrates several methods, including analysis of gaseous pollutant variations, back-trajectory modeling, and AOD observations, to address the complexities inherent in identifying pollution sources in a coastal environment influenced by both continental outflows and local emissions. The methodologies of back-trajectory and AOD analysis by using the Hybrid Single-Particle Lagrangian Integrated Trajectory (HYSPPLIT) model and the Modern-Era Retrospective Analysis for Research and Applications, version 2 (MERRA-2) are shown in Text S1 and S2.

2.3 Observation of gaseous pollutant variation

The atmospheric lifetime of gaseous pollutants varies based on their physical and chemical properties, as well as the complex sources and reactions involved [44]. To identify potential LRT events, we examined the temporal variations of nitrogen oxides (NOx) and O₃. The strong negative correlation between NOx and O₃ diurnal patterns may indicate local sources affecting NOx levels, while a positive correlation during other times may suggest the influence of long-range transported O₃ [45]. Events with minimal diurnal variations in these pollutants were flagged as potential LRT candidates. We defined non-LRT events as those with significant fluctuations in NOx and O₃ levels, characterized by decreased NOx and increased O₃ during the day due to photochemical reactions.

We also analyzed NOx/CO ratios, as lower ratios may indicate LRT events, given the differing atmospheric lifetimes of these species [45]. Carbon monoxide can persist for up to two months during LRT events due to its low reactivity [46], while NOx has a much shorter lifetime (6 to 21 h) and contributes to O₃ formation through reactions with volatile organic compounds (VOCs) [47]. Ground-based trace gas concentration data were obtained from Taiwan EPA monitoring stations in Wanli (25.18° N, 121.69° E), representing LP at Cape Fuguei. Acknowledging the limitations of NOx/CO ratios, particularly in coastal settings, we applied additional criteria to refine our classification.

3 Results and discussion

3.1 LRT events during 2014–2016

Figure 1 illustrates the identification of LRT events based on O₃ and NO_x trends at the Wanli air quality station (20 km away from Cape Fuguei). Under normal conditions, O₃ and NO_x exhibit a clear diurnal anti-correlation due to photochemical reactions. O₃ levels rise during the day as a result of these reactions, while at night, O₃ decreases and NO_x increases owing to the reaction between NO₂ and O₃. This diurnal pattern is typical in the absence of LRT. However, during transboundary pollution events, the diurnal variation of O₃ diminishes, weakening its correlation with NO_x. A significant anti-correlation thus serves as an indicator to differentiate between LRT and LP events. The relationship between the diurnal patterns of NO_x and O₃ has been extensively analyzed using functional data analysis to explore the dynamics of their cycles, interconnections, and varying spatio-temporal patterns [48]. Additionally, Zheng et al. employed the Weather Research and Forecasting-Community Multi-scale Air Quality model and HYSPLIT model to simulate the formation, transport, and sources of ozone. Their findings indicate that ozone precursors emitted from northern China, South Korea, and Japan can be carried via the East China Sea to the southeastern coastal regions of China, resulting in significant transport-related ozone pollution [49].

In Spring 2014, four LRT episodes were noted (Mar. 5–9, Mar. 13–15, Mar. 20–22, and Mar. 30–Apr. 6), as shown in Fig. 1a. These events did not consistently coincide with high pollution levels; for instance, average PM_{2.5} concentrations during Mar. 5–9 and Mar. 20–22 remained below 20 μg m⁻³, likely due to dilution from

clean oceanic air or rainfall. Backward cluster analysis from Mar. 10–16 revealed significant air mass descent, transporting pollutants from the eastern China Sea to Cape Fuguei on Mar. 14–15 (see Fig. 2a and Fig. S2). AOD results, reaching 1.5–2 over the eastern China Sea, further support continuous pollutant transport to southern Taiwan (see Fig. 3). Although the trajectories during Mar. 10 and 12 did not indicate direct transport from high-emission areas, they represented LRT influenced by anthropogenic emissions. The mixing and transformation processes during transport can create distinct air masses, differing from fresh continental and clean marine air. Notably, on Mar. 16, there was a sharp increase in gaseous and particulate pollutants (see Fig. 1a). Analysis of surface and 925 hPa high fields indicated north and southwest (SW) winds (Fig. S3), suggesting a complex mixing event involving both LP and LRT from central to northern Taiwan.

In Autumn 2015, three LRT events were observed (Oct. 25–28, Oct. 31–Nov. 3, and Nov. 9–11), with mean PM_{2.5} concentrations of 24, 17, and 21 μg m⁻³, respectively. A significant pollution episode occurred from Nov. 2–3, supported by backward trajectory analysis showing air mass movement from the eastern China Sea to the site (refer to Fig. 2b and Fig. S4). AOD ranged from 0.5 to 1 (the green area in Fig. S5) confirmed pollutant presence near China’s eastern area. Additionally, Fig. S6 shows high PM_{2.5} accumulation in central Taiwan on Nov. 6–7, driven by a leeward eddy, contributing to pollution on Nov. 8, even during non-LRT days (see Fig. 1b). In Autumn 2016, four more LRT events were recorded (Oct. 29–Nov. 3, Nov. 8–11, Nov. 15–16, and Nov. 22–29). Except for Nov. 15–16, these periods experienced

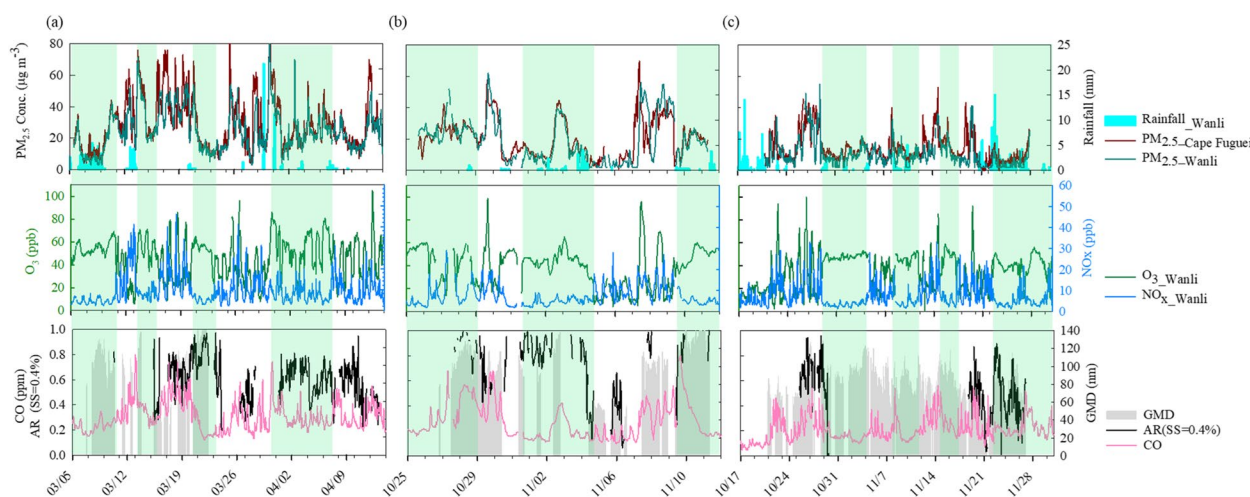


Fig. 1 Temporal variation of PM_{2.5}, rainfall, GMD, AR, NO_x, O₃, CO and wind direction during (a) 2014 Spring, (b) 2015 Autumn, and (c) 2016 Autumn. The green area indicates LRT events

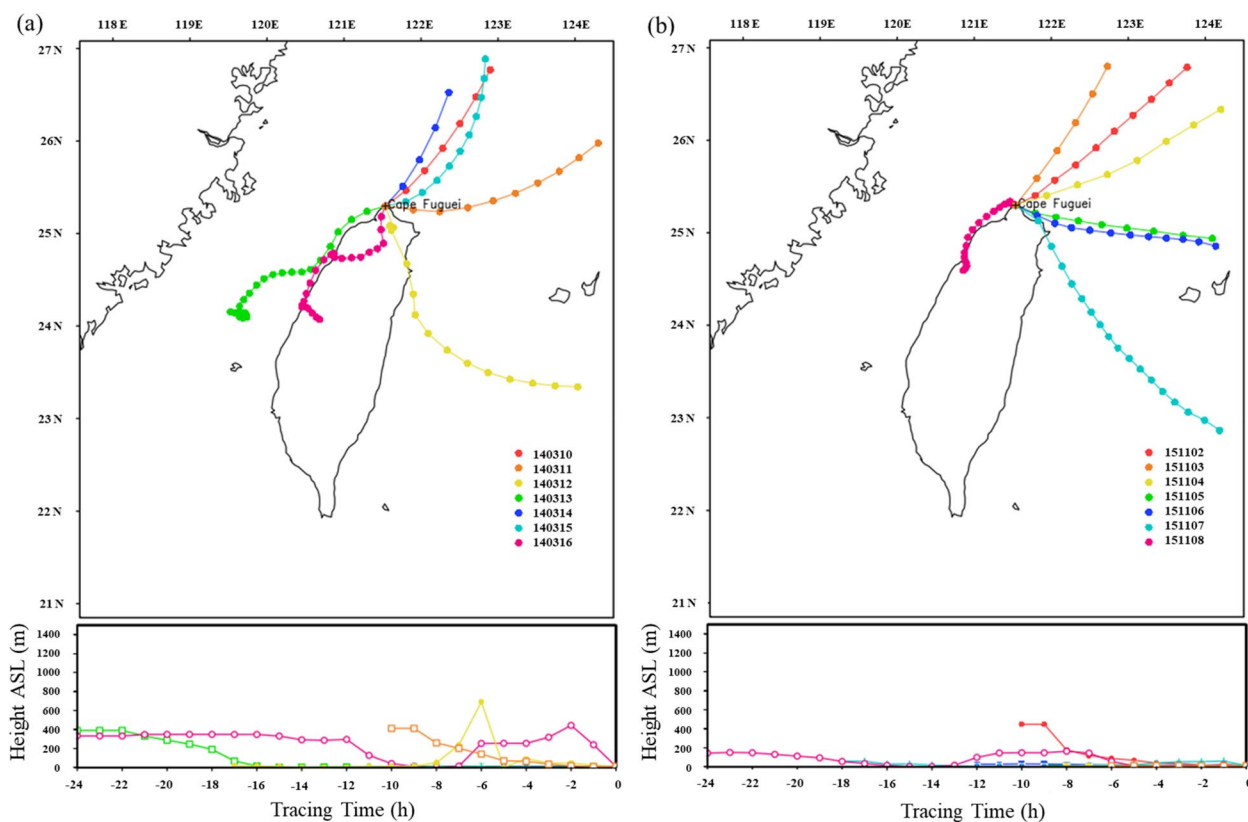


Fig. 2 HYSPLIT backward trajectory in two different years into Cape Fuguei (a) Mar. 10 to Mar. 16, 2014, and (b) Nov. 02 to Nov. 08, 2015

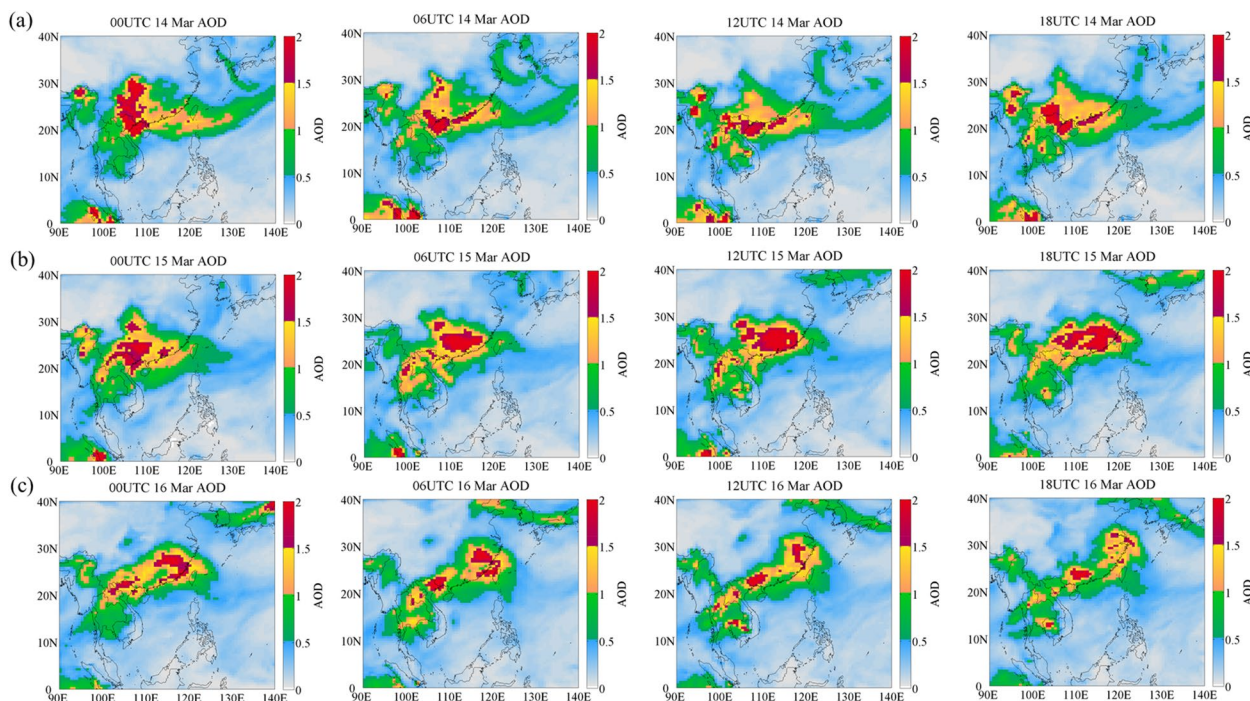


Fig. 3 AOD results of MERRA-2 model during 00UTC, 06UTC, 12UTC, and 18UTC at (a) Mar. 14, (b) Mar. 15, and (c) Mar. 16, 2014

frequent rainfall, resulting in $PM_{2.5}$ concentrations generally below $20 \mu g m^{-3}$ (Fig. 1c).

3.1.1 Categorization of LP and LRT events with NOx/CO correlations

Gaseous pollutants exhibit varying atmospheric lifetimes, which significantly affect their ambient concentrations and dispersion distances. For instance, NOx and CO have lifetimes ranging from 6 to 21 h and approximately 2 months, respectively, making them useful indicators for LP and LRT events [46, 50]. We hypothesized that the NOx/CO ratio during LP events, influenced by SW winds, would be higher than during LRT events associated with NE winds.

Our analysis revealed two distinct clusters in the data (see Fig. 4): one aligned with LP and the other indicating foreign transport. We recognize that the NOx/CO ratio is affected by ventilation conditions, particularly wind speed. Our findings indicate that higher NOx/CO ratios in LP cases often correlate with lower WS, which facilitate the accumulation of locally emitted pollutants. Indeed, the NOx/CO ratios for LP events were consistently higher than those for LRT events in both spring and autumn, supporting our hypothesis. Additionally, LP events were characterized by increased BC mass concentrations.

In contrast, during LRT events with NE winds, the NOx/CO ratio remained around 25, accompanied by relatively low BC emissions. The distribution of the NOx/CO ratio in the autumns of 2015 and 2016 (marked by green dots in Fig. 4) suggests that air mass outflow during the winter/autumn monsoon effectively dilutes local emissions. These relationships between primary emitted NOx, CO, and BC further substantiate our classification of LRT events based on temporal variations in NOx and O_3 . However, distinguishing between LP and LRT events based on gas lifetimes carries inherent uncertainties due to factors like traffic intensity, relative humidity,

temperature, solar radiation, and rainout effects. NOx concentrations suppress the surface O_3 at night and in the early morning, leading to reduced O_3 levels through chemical reactions. Vertical mixing affects the ratio of O_3 precursors in the Planetary Boundary Layer by transporting near-surface O_3 -precursors emissions (NOx and VOCs) to higher levels. While NOx decreases rapidly with altitude, VOCs can persist longer, altering the VOC/NOx ratio and influencing O_3 production [51, 52]. Despite these challenges, our simplified approach provides valuable insights into the seasonal patterns of air pollution at Cape Figuei. Notably, the NOx/CO slope for LP events differed between Spring 2014 and Autumn 2015 but was closer to that of Autumn 2016, potentially reflecting changes in local emission sources and variations in traffic activity.

3.1.2 Case studies of LRT events

The NE wind was generally linked to LRT events, while the SW wind was associated with LP events. This study further examines the effects of transboundary pollution on AR, BC ratio, and GMD over a three-year period. Selected cases from Spring 2014 (Mar. 20–22, CASE I; Mar. 30–Apr. 6, CASE II) and Autumn 2016 (Nov. 22–27, CASE III) are analyzed based on O_3 -NOx temporal variation and NOx/CO ratios.

As shown in Fig. 5a, the AR, BC ratio, and GMD of CASE I ranged from 0.6–1.0, 2–6%, and 80–125 nm, respectively. Additionally, Fig. S7 illustrates an AOD distribution exceeding 1.5 along the southeastern coast of China and mainland Southeast Asia. The increased AR may be attributed to hygroscopic substances carried by oceanic air masses. In contrast, CASE II, depicted in Fig. 5b, exhibited greater fluctuations in AR, BC ratio, and GMD, with values ranging from 0.3–0.8, 1–30%, and 60–125 nm, respectively. High AOD values, as shown in Fig. S8, reached up to 2 during late March and early April, suggesting that transboundary air masses transported

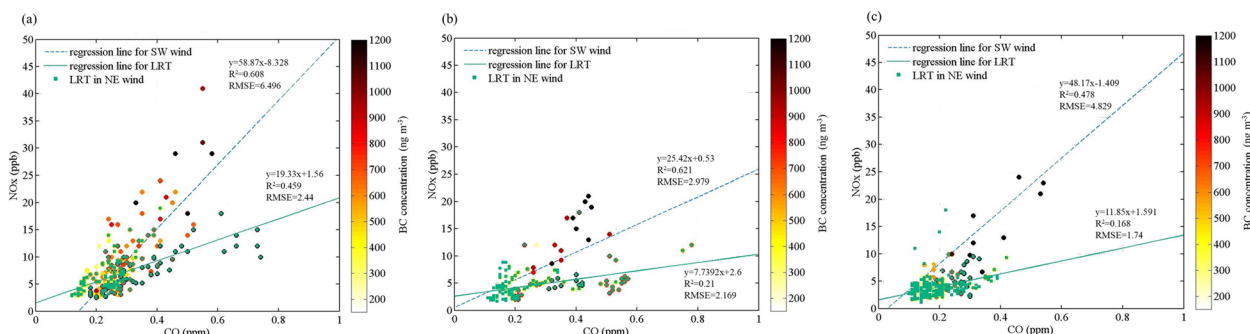


Fig. 4 Correlation between CO and NO_x against BC concentration for determining the LRT in (a) 2014 Spring, (b) 2015 Autumn, and (c) 2016 Autumn. SW: southwest wind, and NE: northeast wind. (RMSE: root mean square deviation)

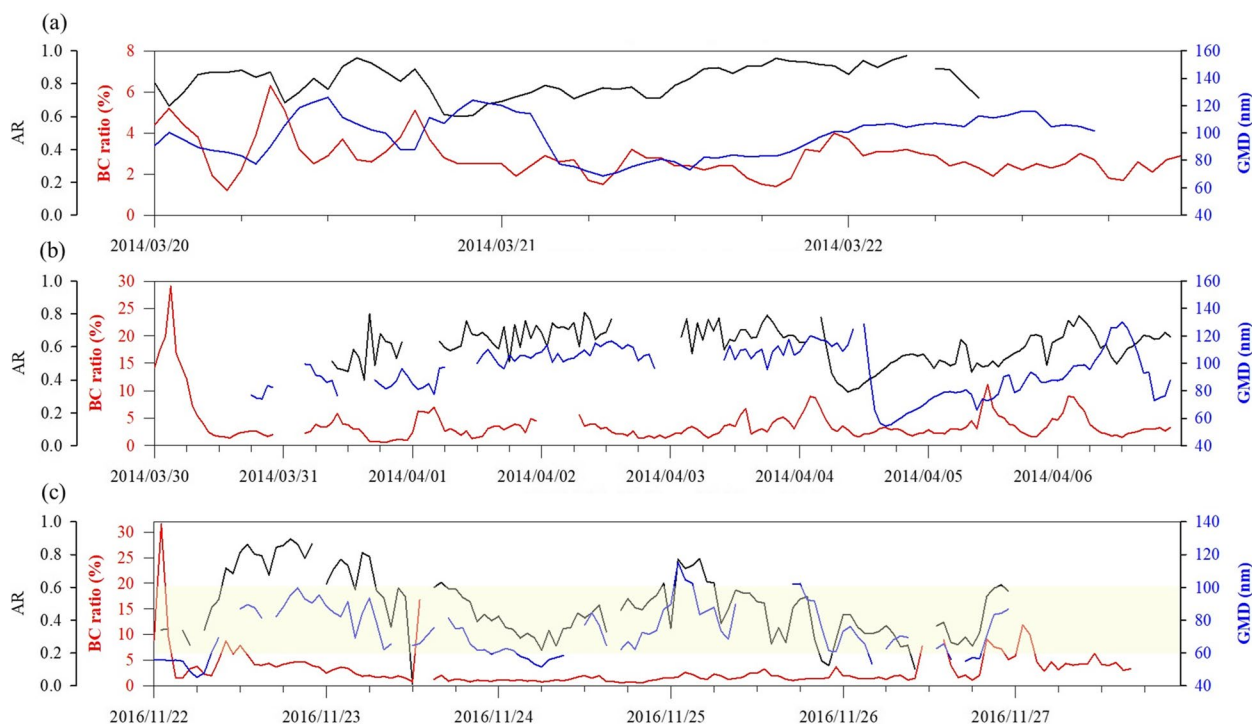


Fig. 5 Time series of AR, BC ratio, and GMD during LRT. (a) CASE I, (b) CASE II, and (c) CASE III

pollutants, evident in the significant peaks of BC ratio and GMD observed.

For CASE III, Fig. 5c indicates a variation between AR and GMD, while the BC ratio consistently remained below 5%. Most air trajectories, illustrated in Fig. S9, originated from the Pacific Ocean, likely enhancing ambient relative humidity and increasing hygroscopic materials. Moreover, the average AOD, shown in Fig. S10, was less than 1, consistent with these observations. The average GMD decreased alongside AR values, ranging from 0.2 to 0.6, as highlighted in the yellow area of Fig. 5c. This suggests that the physical and chemical properties of aerosol particles affecting AR during LRT events are influenced by the winter/autumn monsoon. Thus, seasonal variations in the BC ratio and GMD may serve as indicators of pollution episodes in spring and autumn. Given that CASE III in 2016 was a notably clean LRT event, the following section will focus on comparing LRT events from Spring 2014 and Autumn 2015.

3.2 Analysis of pollutants' characteristics

3.2.1 BC ratio and AR

The relationship between the BC ratio, AR, and wind patterns offers vital insights into pollution events at Cape Fuguei. Figure 6 presents wind rose plots illustrating AR distribution and BC mass concentration for spring 2014 and autumn 2015.

In spring 2014 (see Fig. 6a), dominant eastern winds with high WS were observed. The maximum AR value of 0.8 occurred with WS between 6 to 8 m s⁻¹, primarily from NE and east wind directions. Areas near Cape Fuguei, characterized by robust east and NE winds, frequently exhibited elevated AR values. This suggests that the strong easterly winds may have transported hygroscopic particles, potentially of marine origin, thereby enhancing CCN activity. In contrast, during autumn 2015 (see Fig. 6b), AR values ranged from 0.8 to 0.9 under NE WD, with WS varying from 2 to 8 m s⁻¹. This pattern is attributed to the prevailing winter/autumn monsoon in northern Taiwan. The consistently high AR values across varying WS indicate that the NE monsoon significantly contributes to transporting particles with high CCN potential, likely due to the abundance of sea salt aerosols in marine-influenced air masses.

Notably, BC mass concentrations showed an inverse relationship with AR during both spring and autumn. This trend implies that non-hygroscopic materials like BC may reduce overall AR. The average AR of 0.5–0.8 observed at Cape Fuguei significantly exceeded the AR values of 0.24 ± 0.16, 0.4 ± 0.06, 0.43–0.74, 0.4–0.6, and 0.27–0.36 recorded at various coastal sites, including San Paulo [53], Shanghai [54], west coast of South Korea [55], California [56], and the eastern Arabian Sea near the southern tip of India [57]. This suggests a potentially

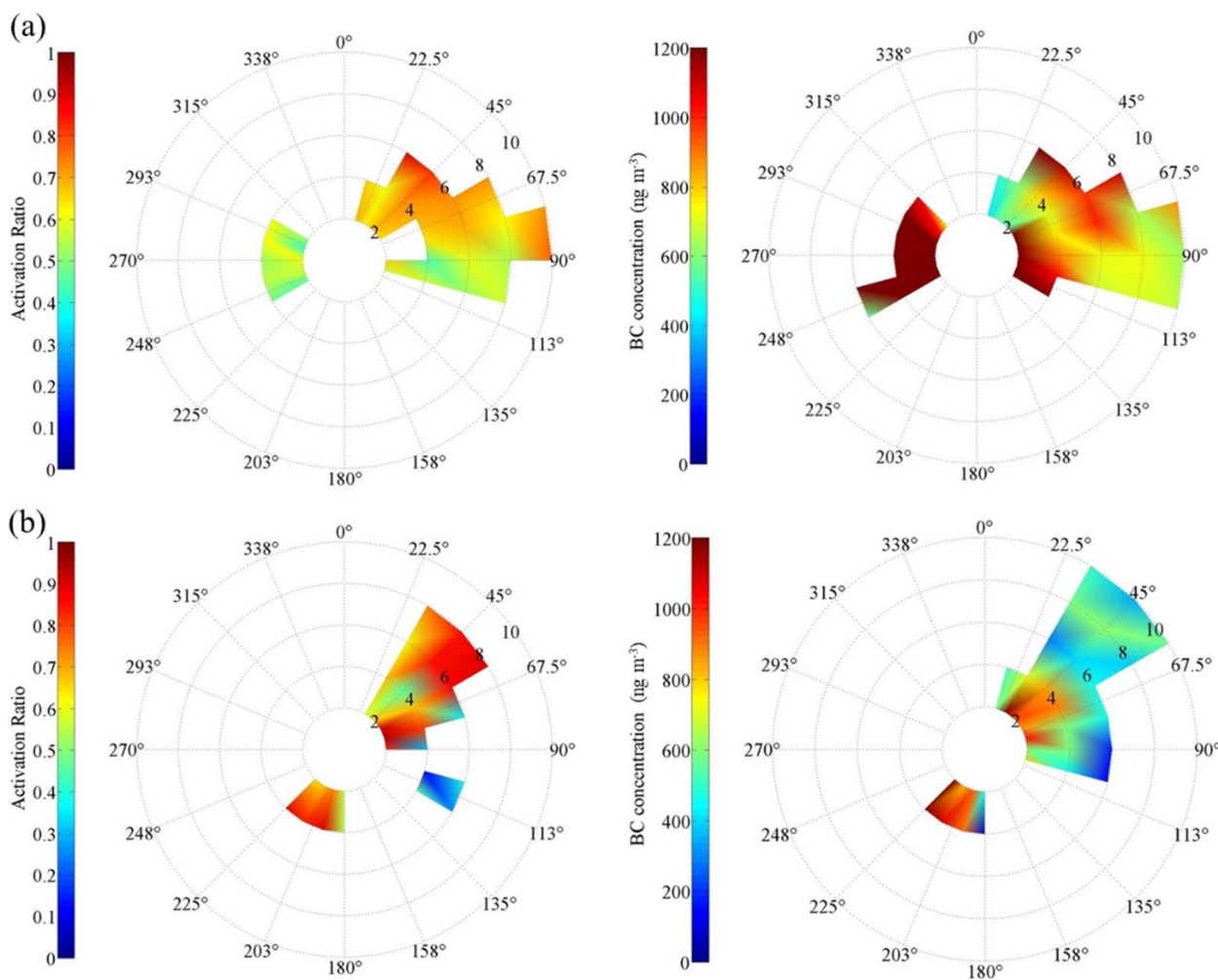


Fig. 6 AR and BC concentration against wind speed and direction at (a) 2014 Spring and (b) 2015 Autumn

higher level of CCN activity in our study area. Further analysis, depicted in Fig. S11 and Table S1, shows that BC ratios during LRT events were generally lower than those during non-LRT events. A negative correlation between BC ratio and AR was noted during both event types in spring 2014 and autumn 2015, highlighting the influence of aerosol composition on CCN activity. An exception occurred in autumn 2016, where a positive correlation between BC ratio and AR emerged, likely due to frequent rainfall that scavenged aerosol particles during the active monsoon season, altering the typical BC and CCN relationship.

3.2.2 Seasonal variations in pollutant characteristics

As shown in Table 1, the mean mass concentrations of PM_{2.5} and BC, PM_{2.5}/PM₁₀ and BC/PM_{2.5} ratios were consistently higher in spring 2014 compared to autumn 2015. This seasonal difference can be attributed to variations in meteorological conditions and pollution sources.

Table 1 Mean values and SD of WS, AR, PM_{2.5}, PM_{2.5}/PM₁₀, BC, and BC/PM_{2.5} during 2014 spring, 2015 autumn, and 2016 autumn

| | 2014 spring | 2015 autumn | 2016 autumn |
|----------------------------------------------------|-------------|-------------|-------------|
| Wind speed (m s ⁻¹) | 4.01 ± 2.83 | 3.88 ± 2.77 | 8.08 ± 4.77 |
| Activation ratio (SS = 0.4%) | 0.61 ± 0.16 | 0.74 ± 0.24 | 0.52 ± 0.21 |
| PM _{2.5} mass conc. (µg m ⁻³) | 29 ± 17 | 21 ± 12 | 14 ± 9 |
| PM _{2.5} /PM ₁₀ ratio (%) | 59 ± 20 | 38 ± 18 | 27 ± 16 |
| BC mass conc. (µg m ⁻³) | 1 ± 0.7 | 0.7 ± 0.5 | 0.7 ± 0.8 |
| BC/PM _{2.5} ratio (%) | 3.5 ± 4.6 | 3.2 ± 4.5 | 5 ± 8.5 |

In Spring 2014, when WS are generally lower, local pollutants may accumulate, leading to higher average PM_{2.5} and BC concentrations reached to 28.8 ± 16.6 µg m⁻³ and 1.01 ± 0.767 µg m⁻³. Generally, the elevated BC mass

concentration observed during periods of lower WS (2–4 m s⁻¹) likely represents LP, possibly generated by ship engine combustion or local burning near Fuji Harbor and carried by SW winds. Ship emissions are a source of various air pollutants, including SO₂, NO_x, and PM_{2.5}, with particulate matter primarily found in smaller sizes under 0.4 μm [58]. This particulate matter mainly consists of elemental carbon, sulfates, and trace metals such as vanadium, nickel, iron, and calcium, and notably, ship emissions contribute to 5.9% of PM_{2.5} concentrations [59]. In contrast, during the autumn seasons of 2015 and 2016, the NE monsoon carried transboundary air masses that effectively diluted and dispersed local pollutants. The continental Asia outflow influenced the chemical composition of PM_{2.5}, although the concentrations of these pollutants tended to decrease due to long-distance transport. Consequently, the average recorded concentrations were notably lower, with PM_{2.5} mass concentrations of 20 ± 12 μg m⁻³ in 2015 and 14 ± 8 μg m⁻³ in 2016. Meanwhile, BC mass concentrations were 0.7 ± 0.5 μg m⁻³ in 2015 and 0.7 ± 0.8 μg m⁻³ in 2016. The discrepancy between seasons further emphasizes the critical role of WS and direction in the distribution and characteristics of pollutants at our study site. The observed differences between spring and autumn LRT events may be partially attributed to seasonal variations in emissions across East Asia. Autumn, being a transitional season, may capture a mix of emission patterns characteristic of both summer and winter, potentially influencing the composition and properties of long-range transported aerosols. This seasonal variability in emissions, coupled with the changing meteorological conditions, likely contributes to the distinct characteristics of LRT events observed in spring versus autumn.

3.2.3 Effect of wind direction on pollutant characteristics

Wind direction significantly influences pollutant characteristics at Cape Fuguei. Figure 7 depicts the relationship between AR, BC ratio, and GMD during LRT events under prevailing NE winds in spring 2014 and autumn 2015.

In spring 2014, LRT events exhibited typical AR values ranging from 0.6 to 0.8, generally surpassing those seen during non-LRT events. However, no significant correlation was found between AR and BC ratio (Fig. S12a) or AR and GMD (Fig. S12b) during LRT, indicating that hygroscopicity was not strongly influenced by particle size. Conversely, autumn 2015 revealed a different pattern: LRT events had higher AR values up to 0.8 to 0.95 compared to non-LRT episodes around 0.5 (Fig. 7c and d), and a positive correlation between AR and GMD was observed (Fig. 7d), with GMD values reaching up to 110 to 130 nm, larger than those (e.g., 90–100 nm) in spring

2014 (Fig. 7b). Notably, this season also showed a negative correlation between GMD and BC ratio (see Fig. S12). These seasonal variations suggest distinct aging processes for transported aerosols, with the stronger positive correlation in autumn indicating that larger particles acted as more effective CCN, likely due to enhanced aging and mixing during transport.

Our analysis of air mass back trajectories over three years indicated multiple transport pathways during winter and autumn, reflecting diverse pollutant sources during LRT events. As shown in Table S2, air masses from coastal China constituted 76% of trajectories in spring 2014, but decreased to 56 and 33% in autumns 2015 and 2016, respectively. This shift likely contributes to the observed differences in aerosol characteristics between spring and autumn. The broader distribution of GMD, coupled with heightened AR values in autumn 2015, indicates a nuanced and heterogeneous aging process (Fig. S13). This rise in GMD can likely be linked to the formation and aggregation of secondary inorganic and organic aerosols onto existing particles, alongside the aging of carbonaceous aerosols, which leads to an increase in particle size. Furthermore, this phenomenon suggests that pollutants from remote sources experience considerable transformations, leading to larger particles and increased CCN activity, especially during LRT events in the autumn. In summary, our findings highlight intricate interactions between local and long-range transported pollutants, demonstrating significant seasonal variations influenced by wind direction at Cape Fuguei.

4 Conclusions

Our study at Cape Fuguei, Taiwan's northernmost point, sheds light on the intricate dynamics of local and LRT air pollution. By analyzing data across three seasons, we identified key differences between LP and LRT events, emphasizing the influence of meteorological conditions on air quality in this coastal area. LRT events, primarily driven by northeastern winds, consistently showed higher AR and lower BC ratios than LP events. This pattern suggests that long-distance air masses undergo transformations that enhance their role as CCN while diluting primary pollutants like BC. Notably, autumn LRT events exhibited a stronger correlation between AR and GMD compared to spring, indicating more significant aerosol aging influenced by winter and autumn monsoon conditions.

Our multi-criteria approach for identifying LRT events—combining gaseous pollutant mixing ratios, back-trajectory analysis, and AOD data—proved effective. We defined LRT events based on criteria such as minimal diurnal variations in NO_x and O₃, low NO_x/CO ratios, back-trajectories from the Asian continent,

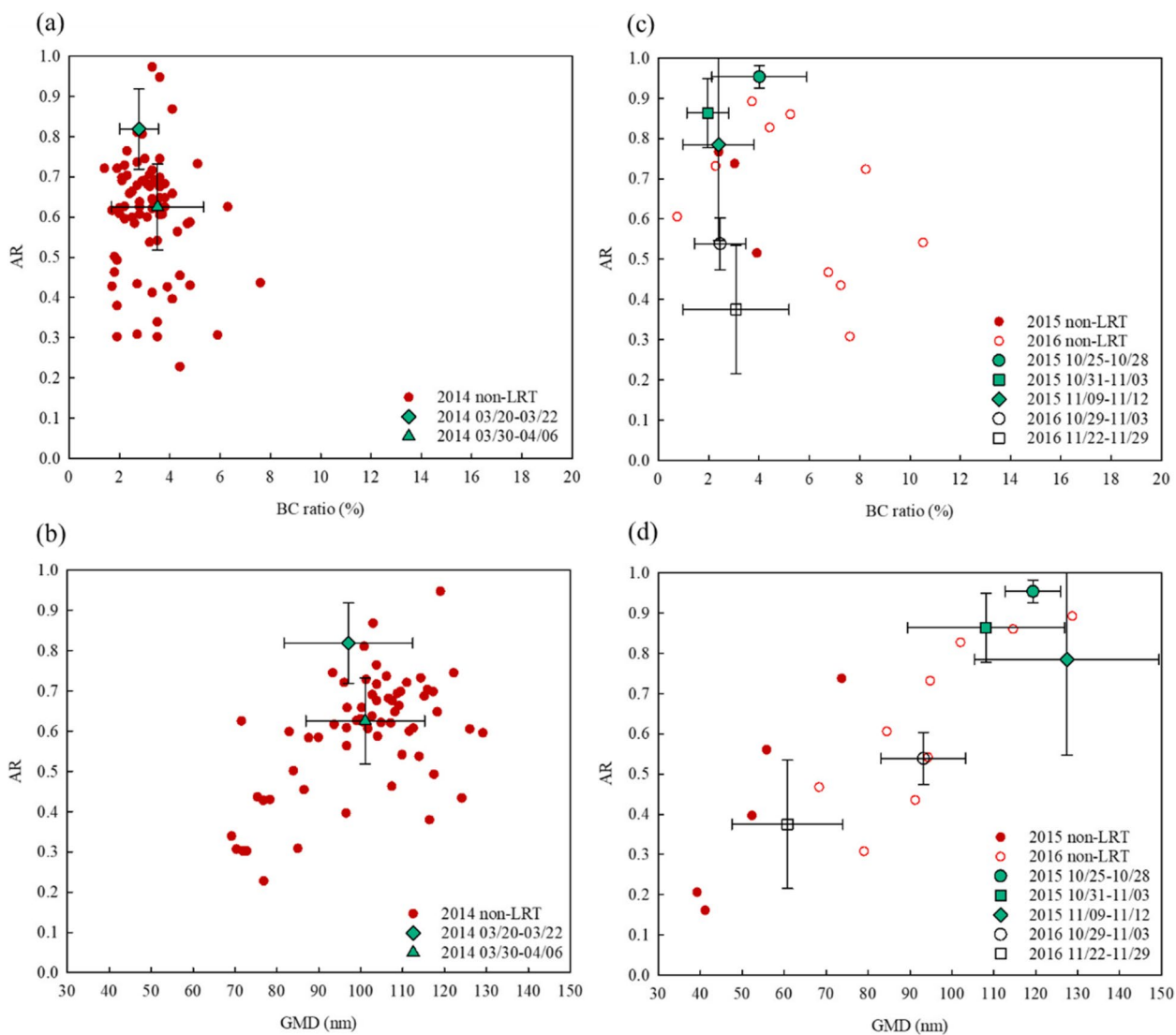


Fig. 7 Correlation of (a) AR with BC ratio in spring, (b) AR with GMD in spring (c) AR with BC ratio in autumn, and (d) AR with GMD in autumn for northeast wind

and increased AOD along the trajectory. Despite our comprehensive approach, the complexities of a coastal environment—such as vertical pollutant transport, local marine sources, and air mass mixing—pose challenges in event classification.

Our findings highlight the necessity of considering large-scale atmospheric circulation patterns in assessing coastal air quality affected by continental outflows. Future research should focus on the chemical composition of aerosols during LRT events and the mechanisms behind seasonal variations. Long-term monitoring will be vital for evaluating trends in LRT’s impact on local air quality amid shifting global emissions. Integrating our insights into regional air quality models could

improve predictive capabilities, particularly in areas experiencing complex transport dynamics. Enhanced identification of LRT events could benefit from on-site measurements of a wider array of chemical species and vertical profile data, reducing uncertainties in understanding local and long-range pollutant interactions.

Supplementary Information

The online version contains supplementary material available at <https://doi.org/10.1186/s42834-025-00250-4>.

Supplementary Material 1.

Declaration of generative AI and AI-assisted technologies in the writing process

During the preparation of this work, the author(s) used OpenAI chatGPT in order to improve readability and language. After using this tool/service, the author(s) reviewed and edited the content as needed and take(s) full responsibility for the content of the publication.

Authors' contributions

Tse-Lun Chen: Conceptualization, Formal analysis, Data curation, Investigation, Writing—original draft. Wei-Jen Hsieh: Methodology, Investigation, Writing—original draft. Hsin-Chih Lai: Methodology, Data curation. Neng-Huei Lin: Conceptualization, Project administration, Supervision. Si-Chee Tsay: Methodology, Supervision. Charles C. K. Chou: Supervision. Ta-Chih Hsiao: Conceptualization, Writing—review & editing, Project administration, Supervision.

Funding

This work was financially supported by the Taiwan Ministry of Science and Technology (now the National Science and Technology Council) under grant No. MOST 105–2119-M-008–014, MOST 106–2111-M-008–009, MOST 107–2628-M-008–002–MY2, and NSTC 113–2222-E-110–003–MY2.

Declarations

Ethics approval and consent to participate

The authors confirm that the study does not involve human or animal subjects.

All the authors mentioned in the manuscript have agreed to authorship and read and approved the manuscript.

Consent for publication

All the authors mentioned in the manuscript approved the version to be published.

Competing interests

The authors declare no competing interests.

Received: 29 November 2024 Accepted: 28 April 2025

Published online: 13 May 2025

References

- Luo M, Hou X, Gu Y, Lau NC, Yim SHL (2018) Trans-boundary air pollution in a city under various atmospheric conditions. *Sci Total Environ.* 618:132–141
- Takemura T, Uno I, Nakajima T, Higurashi A, Sano I (2002) Modeling study of long-range transport of Asian dust and anthropogenic aerosols from East Asia. *Geophys Res Lett.* 29:2158
- Kim CH, Lee HJ, Kang JE, Jo HY, Park SY, Jo YJ et al (2018) Meteorological overview and signatures of long-range transport processes during the MAPS-Seoul 2015 campaign. *Aerosol Air Qual Res.* 18:2173–2184
- Matsuda K, Fujimura Y, Hayashi K, Takahashi A, Nakaya K (2010) Deposition velocity of PM_{2.5} sulfate in the summer above a deciduous forest in central Japan. *Atmos Environ.* 44:4582–4587
- Kaneyasu N, Yamamoto S, Sato K, Takami A, Hayashi M, Hara K et al (2014) Impact of long-range transport of aerosols on the PM_{2.5} composition at a major metropolitan area in the northern Kyushu area of Japan. *Atmos Environ.* 97:416–425
- Chuang MT, Fu JS, Jang CJ, Chan CC, Ni PC, Lee CT (2008) Simulation of long-range transport aerosols from the Asian Continent to Taiwan by a Southward Asian high-pressure system. *Sci Total Environ.* 406:168–179
- Wang SH, Hung WT, Chang SC, Yen MC (2016) Transport characteristics of Chinese haze over Northern Taiwan in winter, 2005–2014. *Atmos Environ.* 126:76–86
- Lin CY, Liu SC, Chou CCK, Huang SJ, Liu CM, Kuo CH et al (2005) Long-range transport of aerosols and their impact on the air quality of Taiwan. *Atmos Environ.* 39:6066–6076
- Hsu CH, Cheng FY (2019) Synoptic weather patterns and associated air pollution in Taiwan. *Aerosol Air Qual Res.* 19:1139–1151
- Tseng YL, Yuan CS, Bagtasa G, Chuang HL, Li TC (2019) Inter-correlation of chemical compositions, transport routes, and source apportionment results of atmospheric PM_{2.5} in southern Taiwan and the northern Philippines. *Aerosol Air Qual Res.* 19:2645–2661
- Ueda S, Nakayama T, Taketani F, Adachi K, Matsuki A, Iwamoto Y et al (2016) Light absorption and morphological properties of soot-containing aerosols observed at an East Asian outflow site, Noto Peninsula, Japan. *Atmos Chem Phys.* 16:2525–2541
- Oh HJ, Min Y, Kim J (2021) Exposure to long-range transported particulate matter and modeling age-related particle deposition. *Environ Sci Pollut R.* 28:69286–69300
- Chou CCK, Lee CT, Cheng MT, Yuan CS, Chen SJ, Wu YL et al (2010) Seasonal variation and spatial distribution of carbonaceous aerosols in Taiwan. *Atmos Chem Phys.* 10:9563–9578
- Pani SK, Lee CT, Chou CCK, Shimada K, Hatakeyama S, Takami A et al (2017) Chemical characterization of wintertime aerosols over islands and mountains in East Asia: impacts of the continental Asian outflow. *Aerosol Air Qual Res.* 17:3006–3036
- Griffith SM, Huang WS, Lin CC, Chen YC, Chang KE, Lin TH et al (2020) Long-range air pollution transport in East Asia during the first week of the COVID-19 lockdown in China. *Sci Total Environ.* 741:140214
- Lai IC, Brimblecombe P (2020) Long-range transport of air pollutants to Taiwan during the COVID-19 lockdown in Hubei Province. *Aerosol Air Qual Res.* 21:200392
- Chuang MT, Chou CCK, Lin NH, Takami A, Hsiao TC, Lin TH et al (2017) A simulation study on PM_{2.5} sources and meteorological characteristics at the northern tip of Taiwan in the early stage of the Asian haze period. *Aerosol Air Qual Res.* 17:3166–3178
- Hung WT, Lu CH, Wang SH, Chen SP, Tsai F, Chou CCK (2019) Investigation of long-range transported PM_{2.5} events over Northern Taiwan during 2005–2015 winter seasons. *Atmos Environ.* 217:116920
- Wang YT, Lin NH, Chang CT, Huang JC, Lin TC (2023) Fog and rain water chemistry in a tea plantation of northern Taiwan. *Environ Sci Pollut R.* 30:96474–96485
- Cheung HC, Chou CCK, Huang WR, Tsai CY (2013) Characterization of ultrafine particle number concentration and new particle formation in an urban environment of Taipei, Taiwan. *Atmos Chem Phys.* 13:8935–8946
- Merikanto J, Spracklen DV, Mann GW, Pickering SJ, Carslaw KS (2009) Impact of nucleation on global CCN. *Atmos Chem Phys.* 9:8601–8616
- Pierce JR, Leaitch WR, Liggio J, Westervelt DM, Wainwright CD, Abbatt JPD et al (2012) Nucleation and condensational growth to CCN sizes during a sustained pristine biogenic SOA event in a forested mountain valley. *Atmos Chem Phys.* 12:3147–3163
- Twomey S (1977) The influence of pollution on the shortwave albedo of clouds. *J Atmos Sci.* 34:1149–1152
- Matsui H, Koike M, Kondo Y, Takegawa N, Fast JD, Poschl U et al (2010) Spatial and temporal variations of aerosols around Beijing in summer 2006: 2. Local and column aerosol optical properties. *J Geophys Res Atmos.* 115:D22207
- Wang J, Cubison MJ, Aiken AC, Jimenez JL, Collins DR (2010) The importance of aerosol mixing state and size-resolved composition on CCN concentration and the variation of the importance with atmospheric aging of aerosols. *Atmos Chem Phys.* 10:7267–7283
- Thalman R, de Sa SS, Palm BB, Barbosa HJM, Pohlker ML, Alexander ML et al (2017) CCN activity and organic hygroscopicity of aerosols downwind of an urban region in central Amazonia: seasonal and diel variations and impact of anthropogenic emissions. *Atmos Chem Phys.* 17:11779–11801
- Rosenfeld D, Lohmann U, Raga GB, O'Dowd CD, Kulmala M, Fuzzi S et al (2008) Flood or drought: how do aerosols affect precipitation? *Science.* 321:1309–1313
- Cheung HC, Chou CCK, Lee CSL, Kuo WC, Chang SC (2020) Hygroscopic properties and cloud condensation nuclei activity of atmospheric aerosols under the influences of Asian continental outflow and new particle formation at a coastal site in eastern Asia. *Atmos Chem Phys.* 20:5911–5922
- Arub Z, Bhandari S, Gani S, Apte JS, Hildebrandt Ruiz L, Habib G (2020) Air mass physiochemical characteristics over New Delhi: impacts on aerosol hygroscopicity and cloud condensation nuclei (CCN) formation. *Atmos Chem Phys.* 20:6953–6971

30. Hudson JG, Noble S (2014) CCN and vertical velocity influences on droplet concentrations and supersaturations in clean and polluted stratus clouds. *J Atmos Sci*. 71:312–331
31. Gunthe SS, Rose D, Su H, Garland RM, Achtert P, Nowak A et al (2011) Cloud condensation nuclei (CCN) from fresh and aged air pollution in the megacity region of Beijing. *Atmos Chem Phys*. 11:11023–11039
32. Bhattu D, Tripathi SN (2015) CCN closure study: Effects of aerosol chemical composition and mixing state. *J Geophys Res Atmos*. 120:766–783
33. Zhang F, Li Y, Li Z, Sun L, Li R, Zhao C et al (2014) Aerosol hygroscopicity and cloud condensation nuclei activity during the AC³Exp campaign: implications for cloud condensation nuclei parameterization. *Atmos Chem Phys*. 14:13423–13437
34. Zhang SL, Ma N, Kecorius S, Wang PC, Hu M, Wang ZB et al (2016) Mixing state of atmospheric particles over the North China Plain. *Atmos Environ*. 125:152–164
35. Xu L, Wu X, Hong Z, Zhang Y, Deng J, Hong Y et al (2019) Composition, mixing state, and size distribution of single submicron particles during pollution episodes in a coastal city in southeast China. *Environ Sci Pollut R*. 26:1464–1473
36. Farmer DK, Cappa CD, Kreidenweis SM (2015) Atmospheric processes and their controlling influence on cloud condensation nuclei activity. *Chem Rev*. 115:4199–4217
37. Seinfeld JH, Bretherton C, Carslaw KS, Coe H, DeMott PJ, Dunlea EJ et al (2016) Improving our fundamental understanding of the role of aerosol–cloud interactions in the climate system. *P Natl Acad Sci USA* 113:5781–5790
38. Zhang F, Ren J, Fan T, Chen L, Xu W, Sun Y et al (2019) Significantly enhanced aerosol CCN activity and number concentrations by nucleation-initiated haze events: a case study in urban Beijing. *J Geophys Res Atmos*. 124:14102–14113
39. Rose D, Nowak A, Achtert P, Wiedensohler A, Hu M, Shao M et al (2010) Cloud condensation nuclei in polluted air and biomass burning smoke near the mega-city Guangzhou, China – Part 1: Size-resolved measurements and implications for the modeling of aerosol particle hygroscopicity and CCN activity. *Atmos Chem Phys*. 10:3365–3383
40. Chuang MT, Lee CT, Hsu HC (2018) Quantifying PM_{2.5} from long-range transport and local pollution in Taiwan during winter monsoon: An efficient estimation method. *J Environ Manage*. 227:10–22
41. Chou CCK, Hsu WC, Chang SY, Chen WN, Chen MJ, Huang WR et al (2017) Seasonality of the mass concentration and chemical composition of aerosols around an urbanized basin in East Asia. *J Geophys Res Atmos*. 122:2026–2042
42. Chou CCK, Lee CT, Yuan CS, Hsu WC, Lin CY, Hsu SC et al (2008) Implications of the chemical transformation of Asian outflow aerosols for the long-range transport of inorganic nitrogen species. *Atmos Environ*. 42:7508–7519
43. Lin CY, Chou CCK, Wang Z, Lung SC, Lee CT, Yuan CS et al (2012) Impact of different transport mechanisms of Asian dust and anthropogenic pollutants to Taiwan. *Atmos Environ*. 60:403–418
44. Seinfeld JH, Pandis SN (2016) *Atmospheric Chemistry and Physics: From Air Pollution to Climate Change*, 3rd edn. John Wiley & Sons, Hoboken
45. Pancholi P, Kumar A, Bikundia DS, Chourasiya S (2018) An observation of seasonal and diurnal behavior of O₃–NO_x relationships and local/regional oxidant (OX = O₃ + NO₂) levels at a semi-arid urban site of western India. *Sustain Environ Res*. 28:79–89
46. Zhang Q, Quan J, Tie X, Li X, Liu Q, Gao Y et al (2015) Effects of meteorology and secondary particle formation on visibility during heavy haze events in Beijing, China. *Sci Total Environ*. 502:578–584
47. Kleinman LI (2005) The dependence of tropospheric ozone production rate on ozone precursors. *Atmos Environ*. 39:575–586
48. Gao HO, Niemeier DA (2008) Using functional data analysis of diurnal ozone and NO_x cycles to inform transportation emissions control. *Transport Res D Tr E*. 13:221–238
49. Zheng Y, Jiang F, Feng S, Cai Z, Shen Y, Ying C et al (2021) Long-range transport of ozone across the eastern China seas: A case study in coastal cities in southeastern China. *Sci Total Environ*. 768:144520
50. Ou Yang CF, Lin YC, Lin NH, Lee CT, Sheu GR, Kam SH et al (2009) Inter-comparison of three instruments for measuring regional background carbon monoxide. *Atmos Environ*. 43:6449–6453
51. Qu K, Yan Y, Wang X, Jin X, Vrekoussis M, Kanakidou M et al (2024) The effect of cross-regional transport on ozone and particulate matter pollution in China: A review of methodology and current knowledge. *Sci Total Environ*. 947:174196
52. Han S, Yao Q, Tie X, Zhang Y, Zhang M, Li P et al (2020) Analysis of surface and vertical measurements of O₃ and its chemical production in the NCP region, China. *Atmos Environ*. 241:117759
53. Souto-Oliveira CE, Andrade MDF, Kumar P, Lopes FJDS, Babinski M, Landulfo E (2016) Effect of vehicular traffic, remote sources and new particle formation on the activation properties of cloud condensation nuclei in the megacity of São Paulo, Brazil. *Atmos Chem Phys*. 16:14635–14656
54. Leng C, Cheng T, Chen J, Zhang R, Tao J, Huang G et al (2013) Measurements of surface cloud condensation nuclei and aerosol activity in downtown Shanghai. *Atmos Environ*. 69:354–361
55. Yum SS, Hudson JG, Song KY, Choi BC (2005) Springtime cloud condensation nuclei concentrations on the west coast of Korea. *Geophys Res Lett*. 32:L09814
56. Furutani H, Dall’osto M, Roberts GC, Prather KA (2008) Assessment of the relative importance of atmospheric aging on CCN activity derived from field observations. *Atmos Environ*. 42:3130–42
57. Jayachandran V, Nair VS, Babu SS (2017) CCN characteristics over a tropical coastal station during south-west monsoon: observations and closure studies. *Atmos Environ*. 164:299–308
58. Rosewig EI, Schade J, Ruser H, Passig J, Zimmermann R, Adam TW (2024) Detection and analysis of ship emissions using single-particle mass spectrometry: A land-based field study in the port of rostock, Germany. *Atmos Environ X*. 24:100302
59. Wang X, Shen Y, Lin Y, Pan J, Zhang Y, Louie PKK et al (2019) Atmospheric pollution from ships and its impact on local air quality at a port site in Shanghai. *Atmos Chem Phys*. 19:6315–6330

Publisher's Note

Springer Nature remains neutral with regard to jurisdictional claims in published maps and institutional affiliations.